ELSEVIER

Journal of Fluids and Structures 22 (2006) 865–876

JOURNAL OF FLUIDS AND STRUCTURES

www.elsevier.com/locate/jfs

Effect of blockage on vortex-induced vibrations at low Reynolds numbers

T.K. Prasanth, S. Behara, S.P. Singh, R. Kumar, S. Mittal*

Department of Aerospace Engineering, Indian Institute of Technology Kanpur, Kanpur, UP 208 016, India

Received 9 October 2005; accepted 13 April 2006
Available online 24 July 2006

Abstract

There have been quite a few studies in the past to investigate the effect of blockage on flow past a stationary cylinder, but very few for the case when the cylinder is vibrating. Compared to a stationary cylinder, a vibrating cylinder is associated with a wider wake and therefore the blockage is expected to play an even more significant role. The effect of blockage on the vortex-induced vibrations of a cylinder at low Re ($\mathrm{Re} \leqslant 150$) is investigated numerically via a stabilized space–time finite element formulation. The cylinder of low nondimensional mass ($m^* = 10$) is free to vibrate in both transverse and in-line directions. Two sets of computations are carried out for each of the cases with 1% and 5% blockage. In the first set of computations the reduced velocity, U^* ($= U/f_n D$, where f_n is the natural frequency of the oscillator, U the free-stream speed, and D the cylinder diameter) is fixed to 4.92 and the effect of Re is studied. In the second set of computations, both Re and U^* are varied. Lock-in is observed for a range of Re. A hysteretic behavior of the cylinder response close to the lower and upper limits of the synchronization/lock-in region is observed for the case with 5% blockage. The flow is associated with a different arrangement of vortices in the wake depending on whether one is on the "increasing Re" or "decreasing Re" branch. However, for the case with 1% blockage, the hysteretic behavior is completely eliminated near the lower Re range of the lock-in. The solutions for the decreasing as well as increasing Re branch are very similar. They are both associated with intermittent switching of the vortex shedding frequency between the structural frequency and the vortex shedding frequency for stationary cylinder. The hysteretic behavior for a range of Re close to the upper limit of the lock-in region is observed for both the low and high blockage.

Keywords: Unsteady flows; Hysteresis; Vortex shedding; Blockage effect; Finite element method

1. Introduction

The flow past a stationary cylinder becomes unsteady for Re beyond 50, approximately. As a result of the unsteady forces, it can undergo vortex-induced vibrations if it is mounted on elastic supports. The flow past a freely vibrating cylinder is associated with various interesting phenomena. Under certain conditions, the cylinder motion causes the vortex shedding to occur at the cylinder vibration frequency. This is referred to as lock-in or synchronization. For a comprehensive review of the research on various aspects of vortex-induced vibration, the reader is referred to the review articles by Williamson and Govardhan (2004) and Bearman (1984).

*Corresponding author. Tel.: +91 0512 2597906; fax: +91 0512 2597561.
E-mail address: smittal@iitk.ac.in (S. Mittal).

0889-9746/$ - see front matter
doi:10.1016/j.jfluidstructs.2006.04.011

Hysteresis in the flow and cylinder response has been reported by various researchers in the past. For example, Feng (1968) observed from his classic free vibrations experiments that for certain flow conditions, a jump to high amplitude oscillation can occur. This jump in the response of the cylinder is associated with a jump in the phase between the aerodynamic forces and cylinder response and is hysteretic in nature. Lock-in and hysteresis in the phase between the aerodynamic forces and cylinder displacement was also reported by Bishop and Hassan (1964) from their forced vibration experiments.

The experiments by Feng (1968) were conducted in air and therefore the mass ratio (m^*) is quite large. Many of the later experiments, for example by Khalak and Williamson (1996), were conducted in water and are of very low normalized mass. Khalak and Williamson (1999) have shown that the flow and response of the cylinder depends to a large extent on the mass-damping parameter, $m^*\zeta$. Two distinct types of response exist. For low $m^*\zeta$, the response consists of three branches: an initial excitation branch, an upper branch and a lower branch. The transition between the initial and upper response branches is hysteretic. Intermittent switching of modes is seen for transition between upper and lower branches. From flow visualizations, they have shown that the initial branch is associated with 2S mode of shedding [the classical Karman street (Williamson and Roshko, 1988)], while the lower branch corresponds to 2P mode. Hysteresis with respect to transition between initial and upper branches is observed for a range of reduced velocities ($U^* = 4.45$–4.70). For high $m^*\zeta$, for example in the experiments by Feng (1968), only two response branches exist: the initial and the lower branch.

Brika and Laneville (1993), in their experimental investigation of vortex-induced vibration of a long flexible circular cylinder with low damping ratios, observed that transverse displacement of the cylinder is hysteretic with variation of flow velocity. Depending on whether the flow velocity is varied progressively or impulsively, two branches of cylinder response exist. The upper branch is realized when the velocity is increased progressively with small increments. In this case, the 2S mode of vortex shedding is observed. The lower branch is obtained when the velocity is either decreased progressively or changed impulsively. This branch is associated with the 2P vortex shedding mode as suggested by Williamson and Roshko (1988) from their experiments for forced oscillation of cylinder. Mittal and Tezduyar (1992) carried out vortex-induced vibration studies for a cylinder restricted to transverse oscillations using finite element method for $290 \leqslant \mathrm{Re} \leqslant 360$. They observed the phenomenon of hysteresis and lock-in in their simulations. They showed, using data for forced oscillations from Koopmann (1967), that hysteresis observed in their computation is a consequence of lock-in. Later, Mittal and Kumar (1999) extended their work to free vibrations of the cylinder in both in-line and cross-flow directions.

The maximum amplitude of transverse oscillations at low Re ($\sim 0.6D$) in the laminar vortex shedding range is significantly smaller than that observed at large Re. In addition, no study till recently had reported the existence of hysteresis in the cylinder response in the laminar vortex shedding regime. Williamson and Govardhan (2004) demonstrated, via compilation of results from the literature for various studies, that in the laminar vortex shedding range, the hysteresis at the low velocity end of synchronization region may exist. Recently, Singh and Mittal (2005) confirmed this via their numerical simulations. They have also shown that in the laminar flow regime, the hysteresis in the flow and response of the cylinder can be observed not only near the low but also near the high end of the lock-in regime. In another study, Mittal and Singh (2005) found that for certain natural frequencies of the spring-mass system, vortex shedding and self-excited vibrations of the cylinder are possible for Re as low as 20.

The effect of blockage on the flow past a stationary cylinder is relatively well known. For example, Kumar and Mittal (2006a,b) investigated the effect of blockage on the critical Re at the onset of the first wake instability. They reported a nonmonotonic variation of the critical Re with blockage. It is found that as the blockage increases, the critical Re for the onset of the instability first decreases and then increases. However, a monotonic increase in the nondimensional shedding frequency at the onset of instability, with increase in blockage, is observed. There have been very few studies to investigate the effect of blockage on flow past an oscillating cylinder. Here, blockage is defined as the ratio of the cylinder diameter to the cross-flow dimension of the wind-tunnel/tow-tank or the computational domain. Our computations of flow past a vibrating cylinder at $\mathrm{Re} = 100$ suggest that even a blockage of 5% may have a significant effect on the flow. Interestingly, a blockage of this order results in fairly acceptable results for the stationary cylinder. Barring the study of Brika and Laneville (1993), the blockage for the investigations discussed above, is larger than 5%. For example, it is 8.3% for Feng (1968), 8.4% for Bishop and Hassan (1964) and 10% for Khalak and Williamson (1996). More details on the blockage used for various experimental studies can be found in the compilation by Norberg (2003). The blockage for the numerical investigations by Singh and Mittal (2005) is 5%, and it is 6.25% for the study by Mittal and Tezduyar (1992). An interesting observation was made by Stansby (1976) in his study for flow past circular cylinders that are subjected to forced transverse oscillations. Two cylinder models were used in the experiments: one with twice the diameter of the other. The vortex shedding frequency locks-in to the cylinder vibration frequency and its sub-multiples. A jump in the phase ϕ between the cylinder displacement and aerodynamic forces is seen for both

cylinder models. However, the hysteretic behavior in the variation of ϕ is seen only for the cylinder with larger diameter, i.e., for the case with high blockage.

In the present work, the effect of location of the lateral boundaries on vortex-induced vibration is investigated. The work is restricted to the low Re flows. First, the effect of the location of the outer computational boundaries for the freely vibrating cylinder in a Re = 100 flow is investigated. To find out the effect of blockage on hysteresis, two sets of computations have been carried out for two values of blockage: 1% and 5%.

2. The governing equations

The flow is assumed to be incompressible. The Navier–Stokes equations are solved in terms of primitive variables: the velocity, u, and the pressure, p. The motion of the cylinder in the two directions along the Cartesian axes is governed by the following equations:

$$\ddot{X} + 4\pi F_n \zeta \dot{X} + (2\pi F_n)^2 X = \frac{2C_D}{\pi m^*} \quad \text{for } (0, T), \tag{1}$$

$$\ddot{Y} + 4\pi F_n \zeta \dot{Y} + (2\pi F_n)^2 Y = \frac{2C_L}{\pi m^*} \quad \text{for } (0, T). \tag{2}$$

Here, F_n is the reduced natural frequency of the oscillator, ζ is the structural damping ratio, m^* is the nondimensional mass of the cylinder, while C_L and C_D are the instantaneous lift and drag coefficients, respectively. The free-stream flow is assumed to be along the x-axis. $\ddot{X}$, $\dot{X}$ and X denote the normalized in-line acceleration, velocity and displacement of the cylinder, while $\ddot{Y}$, $\dot{Y}$ and Y represent the same quantities associated with the cross-flow motion. The displacement and velocity are normalized by the diameter, D of the cylinder and the free-stream speed, U_∞. The reduced natural frequency of the system, F_n is defined as $f_n D/U_\infty$, where f_n is the natural frequency of the oscillator. Another related parameter is the reduced velocity, U^*. It is defined as $U^* = U_\infty/f_n D = 1/F_n$. The nondimensional mass of the cylinder is defined as $m^* = 4m/\pi\rho_\infty D^2$, where m is the dimensional mass of the oscillator per unit length and ρ_∞ is the density of the fluid. The force coefficients are computed by carrying an integration that involves the pressure and viscous stresses around the circumference of the cylinder.

3. The finite element formulation

To accommodate the motion of the cylinder and the deformation of the mesh, the deforming spatial domain/stabilized space–time (DSD/SST) method (Tezduyar et al., 1992a,b) is utilized. Equal-in-order basis functions for velocity and pressure, that are bilinear in space and linear in time, are used. Details on the formulation including those on the stabilization coefficients and its implementation for oscillating cylinders can be found in articles by Tezduyar et al. (1992a–c), Mittal (1992), and Singh and Mittal (2005).

4. Problem description

The cylinder mounted on elastic supports is allowed to vibrate both in the streamwise and transverse directions. The nondimensional mass of the cylinder is $m^* = 10$. To encourage high amplitude oscillations, the structural damping coefficient is set to zero. The Reynolds number, Re is based on the free-stream speed, diameter of the cylinder and viscosity of the fluid. The springs in both the transverse and in-line directions are assumed to be linear and with identical stiffness.

It was pointed out by Singh and Mittal (2005) that, for a given spring-mass system, F_n and Re are not independent parameters. It can be seen from Eqs. (1) and (2) that F_n ($= 1/U^*$) varies inversely with Re. However, in a numerical environment, the two can be varied independently. Singh and Mittal (2005) carried out two sets of computations: in the first set of computations, Re was set to 100 and the reduced velocity, U^* was varied. The maximum amplitude for transverse oscillations are observed for $U^* \sim 4.75$. The second set of computations were carried out for a fixed value of $U^* (= 4.92)$ with the objective of investigating the effect of Re when the cylinder vibrates at, approximately, its maximum amplitude. In both cases, hysteresis was observed for a range of Re close to the limits of the synchronization region.

The computations by Singh and Mittal (2005) are for 5% blockage, that we now believe is too high to model unbounded flows for oscillating bluff bodies, at least for low Re. In the present work, we first investigate the effect of blockage for the case when U^* is set to a fixed value (= 4.92) and the computations are carried out for various Re. In the second study, we investigate a certain spring-mass oscillator with fixed f_n, i.e., U^* varies linearly with Re.

4.1. Finite element mesh and mesh moving scheme

The cylinder resides in a rectangular computational domain whose upstream and downstream boundaries are located at distance L_u and L_d from the center of the cylinder. The lateral boundaries are separated by a distance H. Fig. 1 shows a typical finite element mesh used for the computations. The blockage ratio, B is defined as $B = D/H$. For the mesh shown in Fig. 1, B is 5%. The mesh moving scheme has been designed such that the mesh in the square box around the cylinder moves along with it as a rigid body. The location of the outer boundary is fixed. As a result, the movement of the cylinder causes deformation of the mesh points lying between the square region and the outer boundary. This kind of mesh movement is expected to lead to almost no projection errors in the flow close to the cylinder. This scheme has been used in our earlier work; for example, in Mittal and Kumar (1999) for single cylinder and in Mittal and Kumar (2001) for a pair of cylinders.

4.2. Boundary conditions

The no-slip condition is applied on the velocity at the cylinder boundary. The location of the cylinder and its own velocity are updated at each nonlinear interaction by solving the equations of motion for the oscillator. Free-stream values are assigned for the velocity at the upstream boundary and the viscous stress vector is set to zero at the downstream boundary. On the upper and lower boundaries, the component of the velocity normal to and the component of the stress vector along the boundaries are prescribed zero value.

5. Results

Computations are carried out for two values of blockage: $B = 5\%$ $(H/D = 20)$ and $B = 1\%$ $(H/D = 100)$. The mesh employed for the 5% blockage case consists of 7437 nodes and 7236 elements, while that for $B = 1\%$ consists of 26 020 nodes and 25 650 elements. Equal-in-order basis functions for velocity and pressure, that are bilinear in space and linear

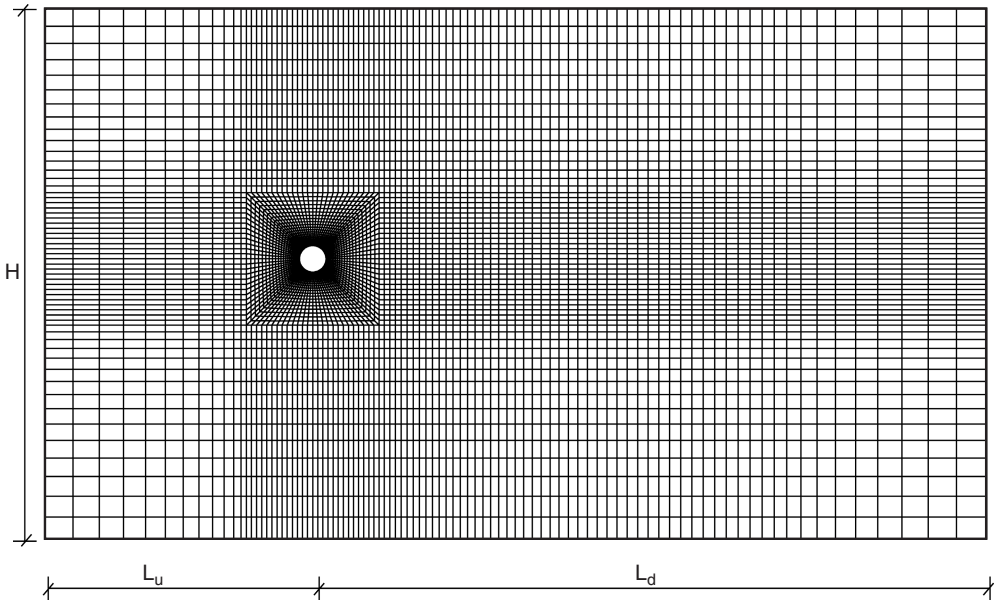

Fig. 1. Vortex-induced vibrations: the finite element mesh utilized for the computations with 5% blockage. It consists of 7437 nodes and 7236 quadrilateral elements.

in time, are used. A $2 \times 2 \times 2$ Gaussian quadrature is employed for numerical integration. The nonlinear equation systems resulting from the finite-element discretization of the flow equations are solved using the Generalized Minimal RESidual (GMRES) technique in conjunction with diagonal preconditioners.

In all the figures for the vorticity field presented in this article, a gray scale based on the magnitude of vorticity is used for shading. The darker shades of gray represent higher values of vorticity. To differentiate between positive and negative values, iso-vorticity contours are also shown. Black-colored contour lines represent negative, while the white-colored lines show positive values of the vorticity field.

5.1. *Mesh convergence study* (Re = 100, $U^* = 4.92$)

Two meshes are utilized: M7k and M18k. The domain size for the two cases is identical. For the stationary cylinder, the results from the two meshes are in very good agreement (Singh and Mittal, 2005). The summary of the aerodynamic coefficients for the cylinder and its response to the unsteady fluid forces for the two meshes is shown in Table 1. It can be observed that the two meshes give very similar results. Amongst all the quantities, the maximum difference between the values from the two meshes is for the amplitude of lift coefficient. However, this is a mere 3%, approximately. Interestingly, even though the amplitudes of lift coefficient from the two meshes are slightly different, the cylinder response is virtually same. More details on the mesh resolution study can be found in Singh and Mittal (2005).

5.2. *Effect of L_d/D, the location of downstream boundary* (Re = 100, $U^* = 4.92$)

Computations are carried out for three locations of the downstream boundary. The mesh used for $L_d/D = 25.5$ case consists of 18 220 nodes and 17 904 elements, while that for $L_d/D = 50$ consists of 24 100 nodes and 23 714 elements. There are 29 980 nodes and 29 524 elements in the mesh employed for the $L_d/D = 100$ case. The upstream ($L_u/D = 10$) and transverse ($H/D = 20$) locations of the domain boundary are identical for these cases. The initial condition for all the three cases is the steady-state solution for flow past a stationary cylinder. The results are summarized in Table 2. It is clear from this table that the location of the downstream boundary beyond $25.5D$ does not affect the results for the cylinder oscillations significantly. Vorticity fields corresponding to instants of maximum lift coefficient are shown in Fig. 2. For $L_d = 100$ the far wake exhibits a secondary frequency (Cimbala et al., 1988). However, this does not seem to affect the near-wake dynamics.

Table 1
Vortex-induced vibrations for $U^* = 4.92$ and Re = 100: summary of the aerodynamic coefficients and response of the cylinder for two different finite element meshes

Mesh	Nodes	St	$\left(\frac{Y}{D}\right)_{\max}$	$\left(\frac{X}{D}\right)_{\text{r.m.s.}}$	$\overline{\left(\frac{X}{D}\right)}$	$C_{L\max}$	$C_{D\max}$	$C_{D\text{r.m.s.}}$	$\overline{C_D}$
M7k	7437	0.201	0.57	0.01	0.09	0.96	3.01	0.42	2.39
M18k	26 020	0.200	0.57	0.01	0.09	0.93	3.01	0.42	2.38

For both the cases, $L_d/D = 25.5$, $L_u/D = 10$ and $B = 5\%$. St is the Strouhal number, $\overline{C_D}$ the mean drag coefficient, $C_{D\text{r.m.s.}}$ the r.m.s. value of the lift coefficient, and $C_{L\max}$ and $C_{D\max}$ are the maximum values of the lift and drag coefficients, respectively. $(X/D)_{\text{r.m.s.}}$ and $\overline{(X/D)}$ represent the r.m.s. and mean value of the in-line oscillations while $(Y/D)_{\max}$ is the maximum value of the amplitude of transverse oscillations.

Table 2
Vortex-induced vibrations for $U^* = 4.92$ and Re = 100: summary of the aerodynamic coefficients and response of the cylinder for three locations of the downstream boundary

$\frac{L_d}{D}$	St	$\left(\frac{Y}{D}\right)_{\max}$	$\left(\frac{X}{D}\right)_{\text{r.m.s.}}$	$\overline{\left(\frac{X}{D}\right)}$	$C_{L\max}$	$C_{D\max}$	$C_{D\text{r.m.s.}}$	$\overline{C_D}$
25.5	0.200	0.57	0.01	0.09	0.93	3.01	0.42	2.38
50	0.200	0.57	0.01	0.09	0.89	3.09	0.42	2.38
100	0.201	0.56	0.01	0.09	0.88	2.99	0.42	2.38

For all the cases, $L_u/D = 10$ and $B = 5\%$.

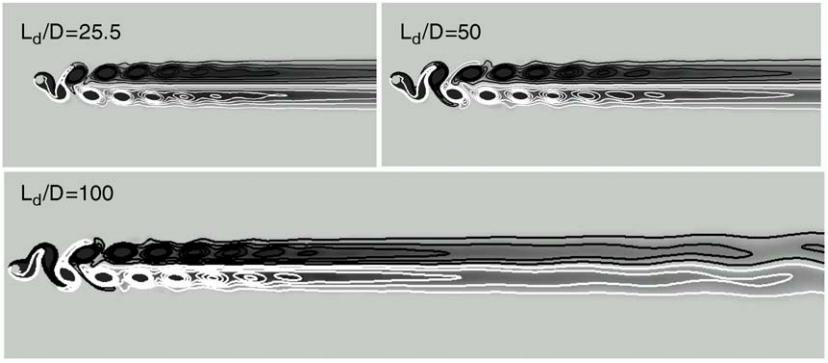

Fig. 2. Vortex-induced vibrations for $U^* = 4.92$ and $\mathrm{Re} = 100$: the instantaneous vorticity field for various normalized downstream size L_d/D of the domain. The pictures correspond to the instant when the lift coefficient achieves its peak value.

Table 3
Vortex-induced vibrations for $U^* = 4.92$ and $\mathrm{Re} = 100$: summary of the aerodynamic coefficients and response of the cylinder for three cases of blockage

B (%)	St	$\left(\frac{Y}{D}\right)_{\max}$	$\left(\frac{X}{D}\right)_{\text{r.m.s.}}$	$\overline{\left(\frac{X}{D}\right)}$	$C_{L\max}$	$C_{D\max}$	$C_{D\text{r.m.s.}}$	$\overline{C_D}$
5	0.200	0.57	0.01	0.09	0.89	3.09	0.42	2.38
2.5	0.213	0.59	0.01	0.08	1.41	2.88	0.42	2.27
1	0.200	0.58	0.02	0.06	2.23	2.74	0.38	1.67

The location of the downstream boundary, for all the cases, corresponds to $L_d/D = 50$.

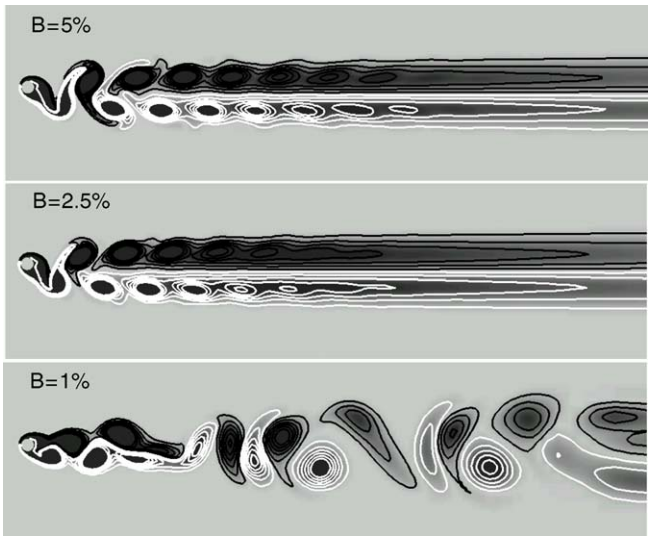

Fig. 3. Vortex-induced vibrations for $U^* = 4.92$ and $\mathrm{Re} = 100$: instantaneous vorticity field for various blockage ratios. The vorticity fields correspond to the instant when the lift coefficient achieves its peak value.

5.3. *Effect of H/D, the lateral width of the domain* ($\mathrm{Re} = 100, U^* = 4.92$)

Three cases of blockage, $B = 5\%$, 2.5% and 1%, are studied to see the effect on vortex-induced vibrations. The summary of results obtained from the three computations is given in Table 3. The mesh used for the $B = 5\%$ case consists of 24 100 nodes and 23 714 elements while that for the $B = 2.5\%$ case consists of 23 644 nodes and 23 280 elements. There are 24 604 nodes and 24 230 elements in the mesh employed for the $B = 1\%$ case. The location of the downstream boundary is same for all the cases. It is seen from Fig. 3 that the wake structure for the 1% blockage is significantly different from that for the other two cases. For $B = 5\%$ and 2.5% the C(2S) mode of shedding is observed. This mode of shedding is similar to 2S, but the vortices coalesce in the wake slightly downstream of the cylinder. It appears that, compared to an unbounded flow, the proximity of the lateral boundaries to the cylinder causes suppression of possible modes in the wake. Compared to the high blockage cases, the aerodynamic coefficients are also quite different for $B = 1\%$. It is interesting to note that even though there is a significant difference in the maximum value of lift coefficient observed for low blockage and high blockage, the maximum transverse oscillation amplitude is virtually the same in all cases. This study is our motivation for investigating the blockage effects in detail.

5.4. *Vortex-induced vibrations: $U^* = 4.92$, variation with* Re

5.4.1. *Overview of the cylinder response*

Fig. 4 shows the variation of the normalized maximum amplitude of the cylinder response in the transverse and in-line directions with Re for blockage ratios, 1% and 5%. The variation of the lift and drag coefficients is also shown in the figure. The phenomenon of hysteresis is seen only for the 5% blockage; the range of Re over which hysteresis takes place is ~76.5–84.5. For the low blockage case the solutions for both the increasing and decreasing Re are same. From Fig. 4 it is observed that, compared to the high blockage, the jump in the amplitude of cylinder response is delayed to a larger Re for the low blockage. In addition, the jump for the high blockage is much sharper than that for the low blockage. Compared to the variation of cylinder response, the variation of the lift coefficient is significantly different for the two cases. For the high blockage, after reaching the peak, the maximum value of the lift coefficient decreases immediately with Re. However, for the low blockage case, it sustains a high value for a range of Re, before suffering another jump to a lower value. Within this range, the cylinder response switches intermittently between low and high amplitude oscillations.

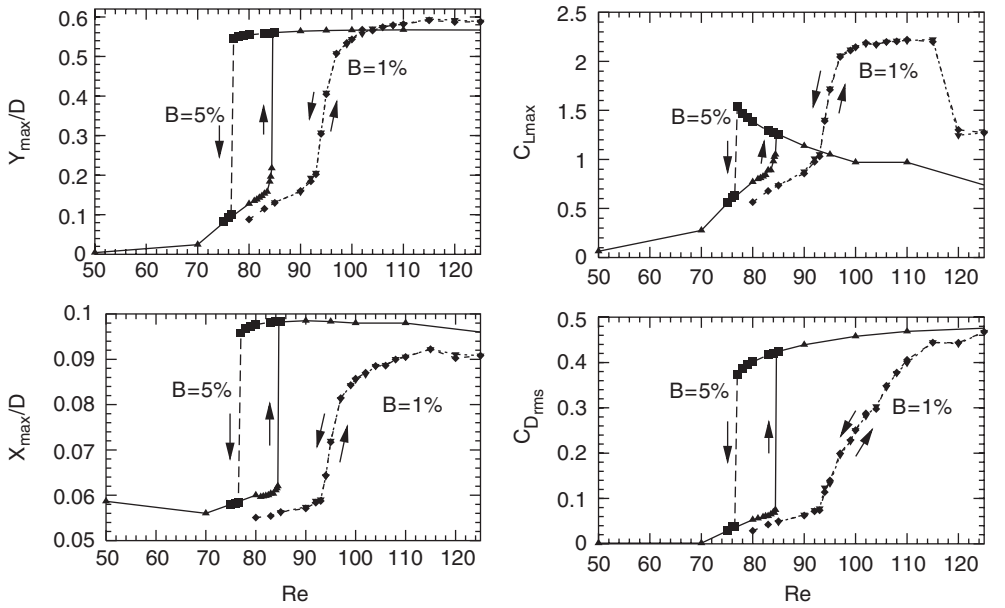

Fig. 4. Vortex-induced vibrations for $U^* = 4.92$: variation of maximum amplitude/r.m.s. value of the cylinder response and the aerodynamic coefficients for two different blockage ratios with Re.

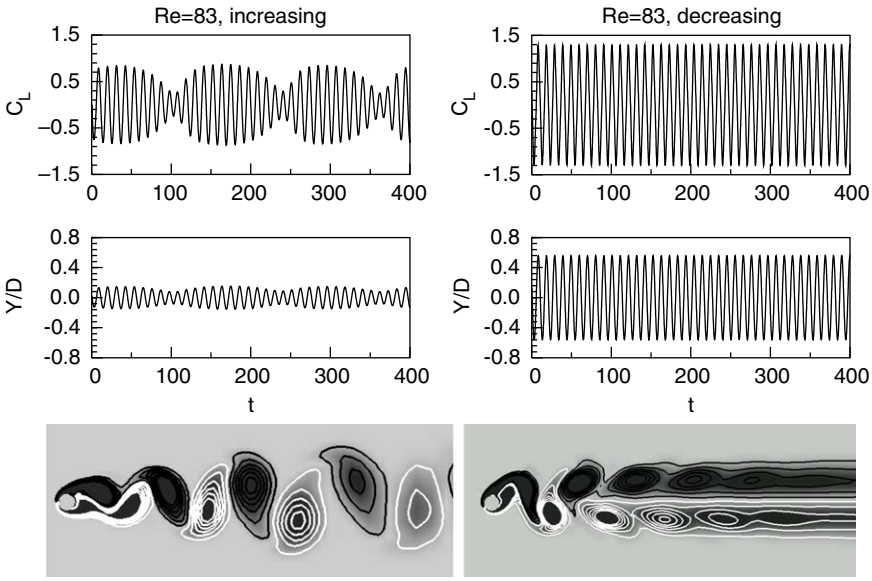

Fig. 5. Vortex-induced vibrations with 5% blockage for $U^* = 4.92$ and $\mathrm{Re} = 83$: time histories of the cylinder response and aerodynamic coefficients and the vorticity field for increasing and decreasing Re.

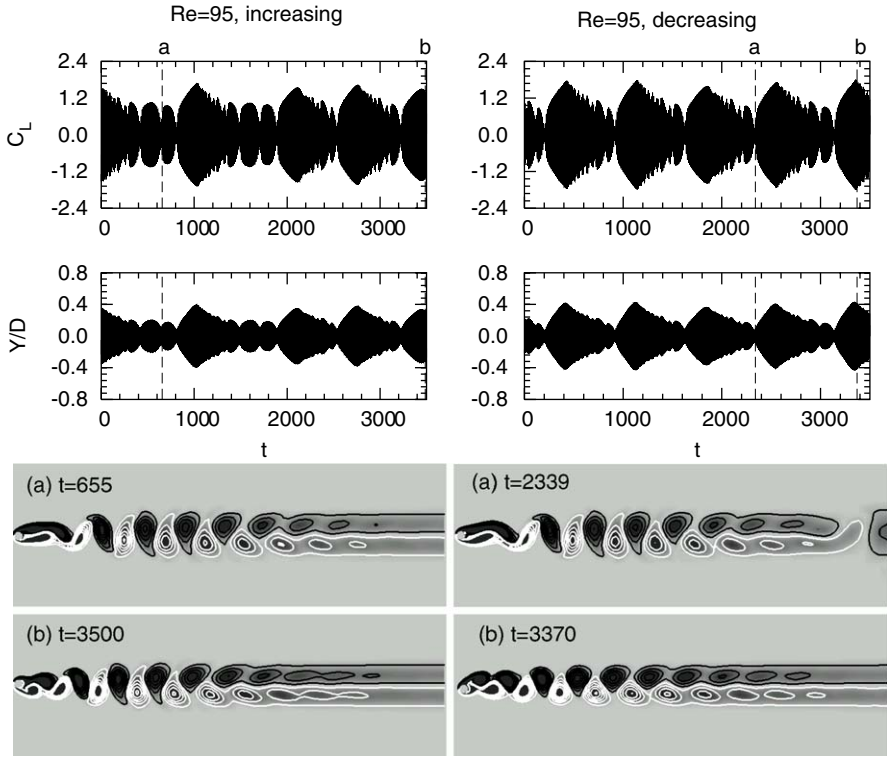

Fig. 6. Vortex-induced vibrations with 1% blockage for $U^* = 4.92$ and $\mathrm{Re} = 95$: time histories of the cylinder response and aerodynamic coefficients and the vorticity field for increasing and decreasing Re. The flow fields at different times: (a) during the low amplitude response; (b) for large amplitude response of the cylinder.

5.4.2. Flow near the jump: high blockage

In an attempt to further understand the effect of blockage, we look at time histories and the flow corresponding to some values of Re near the jump. Fig. 5 shows the time histories of the lift coefficient and the cylinder response for the increasing as well as decreasing Re for 5% blockage at $\mathrm{Re} = 83$. While a low amplitude response is observed for the increasing Re branch, high amplitude vibration is observed for the solution corresponding to the decreasing Re branch. Beats are clearly observed for the low amplitude solution. In this case, the vortex shedding frequency is very close to that for the stationary cylinder. The mode of shedding is 2S. For the decreasing Re case, lock-in is observed. In this case, the vortex shedding frequency is very close to the natural frequency of the oscillator and the mode of shedding is C(2S).

5.4.3. Flow near the jump: low blockage

Fig. 6 shows the time histories of the aerodynamic coefficients and the cylinder response for the increasing as well as decreasing Re for low blockage ($B = 1\%$) at $\mathrm{Re} = 95$. The time histories and the flows for both increasing and decreasing Re are very similar. Figs. 7 and 8 show similar plots for $\mathrm{Re} = 108$ and 125, respectively. From Fig. 4 it is seen that while $\mathrm{Re} = 108$ corresponds to the point just before the cylinder achieves maximum vibration amplitude; $\mathrm{Re} = 125$ is well beyond the jump. It is clear from these figures that for the range of Re when the cylinder response increases from a low to high amplitude, for each Re within this range, the flow displays an intermittent switching between two modes of vortex shedding. A frequency analysis of cylinder response for $\mathrm{Re} = 108$ shows the intermittent switching of the vortex shedding frequency between the value for a stationary cylinder and the structural frequency of the spring-mass

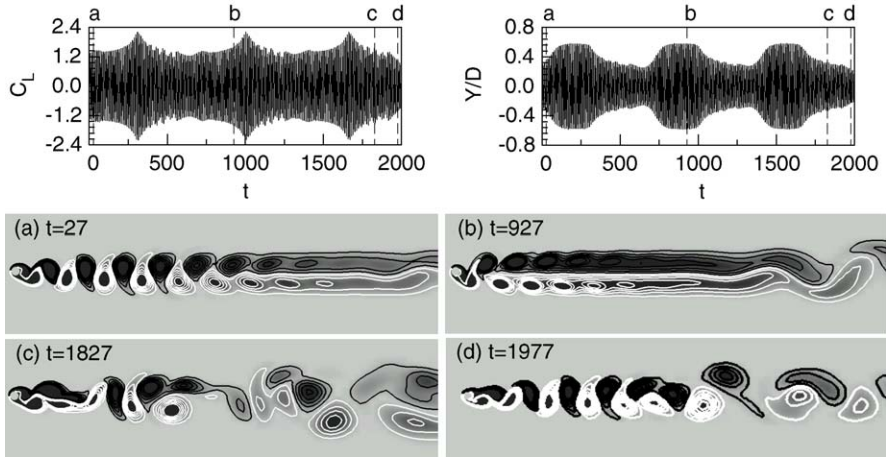

Fig. 7. Vortex-induced vibrations with 1% blockage for $U^* = 4.92$ and $\mathrm{Re} = 108$: time histories of the cylinder response and aerodynamic coefficients and the vorticity field at various times.

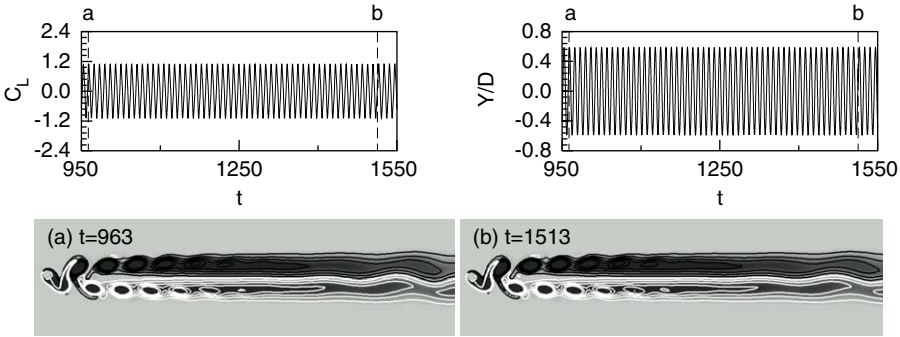

Fig. 8. Vortex-induced vibrations with 1% blockage for $U^* = 4.92$ and $\mathrm{Re} = 125$: time histories of the cylinder response and aerodynamic coefficients and the vorticity field at various times.

system. From the flow pictures at various time instants, it is observed that the high amplitude response corresponds to the C(2S) mode, while the low amplitude response corresponds to the 2S mode. The longitudinal spacing between the vortices is related to the vortex shedding frequency. We also observe that as the Re increases and the maximum amplitude of the cylinder approaches the peak amplitude, the flow stays increasingly longer in the C(2S) mode. Eventually, only the C(2S) mode is observed (for example, at Re = 125).

5.5. *Vortex-induced vibrations: both U^* and* Re *varying*

We now present results for the case where f_n is fixed and therefore, U^* varies inversely with Re. Unlike the previous case, the present case is closer to a physical experiment. Fig. 9 shows the variation of maximum amplitude of cross-flow oscillations and the lift coefficient with Re for 1% and 5% blockage. While in the case with $U^* = 4.92$ where the maximum amplitude of the cylinder response is constant beyond the jump, it varies significantly in the present case. The cylinder response and the fluid forces are associated with jumps at both the upper and lower limits of the Re range of the lock-in region. The behavior near the first jump at the lower Re limit of the lock-in is very similar to the study for $U^* = 4.92$. Hysteresis is observed only for the 5% blockage. However, the hysteresis at the higher Re limit of the synchronization region is observed for both low as well as high blockage. As in the previous study, even though the amplitudes of the cylinder response for the two blockages are quite comparable, the aerodynamic forces are not. More details for this study will be presented in a later paper.

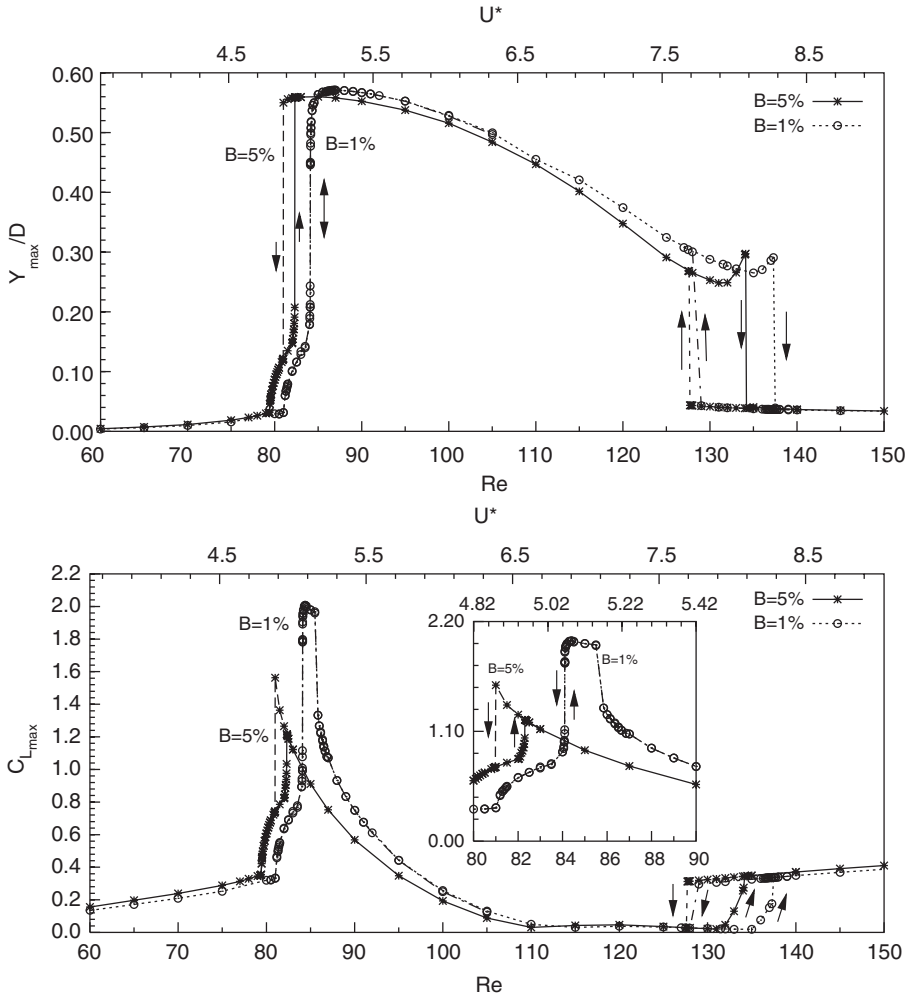

Fig. 9. Vortex-induced vibrations for varying Re and U^*: variation of the cylinder response and the lift coefficient for 1% and 5% blockage.

6. Conclusions

The effect of the location of computational boundaries on the incompressible flow past a freely oscillating cylinder at low Re has been investigated using a stabilized finite element method. It is found that there is no significant effect of the location of the downstream boundary beyond $25.5D$ on the near wake flow and the cylinder response. However, the blockage effects are significant. Even though 5% blockage produces reasonably accurate solutions for unbounded flow past a stationary cylinder, it leads to significantly different solutions for free vibrations. Two sets of computations are carried out. In the first set, the reduced velocity is fixed to $U^* = 4.92$ and the Reynolds number ($60 < \mathrm{Re} < 125$) is varied. In the second set of computations, both reduced velocity and Reynolds number are varied. It is found that with 5% blockage, a hysteretic behavior close to the lower and upper limits of the synchronization/lock-in region can occur depending on whether one is on the "increasing Re" or "decreasing Re" branch. The two solutions are associated with different arrangement of vortices in the wake. For the case with 1% blockage, the hysteretic behavior, near the lower limit of the lock-in region, is completely eliminated. The solutions of the decreasing as well as increasing Re branch appear very similar. At each Re, an intermittent switching of the vortex shedding frequency between the structural frequency and the shedding frequency for a stationary cylinder is observed. Unlike the first jump, the jump in the cylinder response at the upper Re end of the lock-in region is hysteretic irrespective of the degree of blockage. These computations demonstrate the significance of blockage in investigating bluff body flows at low Re. The effect of blockage at moderate to high Re remains to be investigated.

Acknowledgment

This work was partially supported by Department of Science and Technology, India.

References

Bearman, P.W., 1984. Vortex shedding from oscillating bluff bodies. Annual Review of Fluid Mechanics 16, 195–222.

Bishop, R.E.D., Hassan, A.Y., 1964. The lift and drag forces on a circular cylinder oscillating in a flowing fluid. Proceedings of Royal Society of London, Series A 277, 51–75.

Brika, D., Laneville, A., 1993. Vortex-induced vibrations of a long flexible circular cylinder. Journal of Fluid Mechanics 250, 481–508.

Cimbala, J.M., Gharib, H.M., Roshko, A., 1988. Large structure in the far wakes of two-dimensional bluff bodies. Journal of Fluid Mechanics 190, 265–298.

Feng, C.C., 1968. The measurement of vortex-induced effects in flow past a stationary and oscillating circular cylinder and d-section cylinders. Master's Thesis, University of British Columbia, Vancouver, Canada.

Khalak, A., Williamson, C.H.K., 1996. Dynamics of a hydroelastic cylinder with very low mass and damping. Journal of Fluids and Structures 10, 455–472.

Khalak, A., Williamson, C.H.K., 1999. Motions, forces and mode transitions in vortex-induced vibrations at low mass damping. Journal of Fluids and Structures 13, 813–851.

Koopmann, G.H., 1967. The vortex wakes of vibrating cylinders at low Reynolds numbers. Journal of Fluid Mechanics 28, 501–512.

Kumar, B., Mittal, S., 2006a. Effect of blockage on critical parameters for flow past a circular cylinder at low Reynolds number. International Journal for Numerical Methods in Fluids 50, 987–1001.

Kumar, B., Mittal, S., 2006b. Prediction of the critical Reynolds number for flow past a circular cylinder. Computer Methods in Applied Mechanics and Engineering, accepted for publication.

Mittal, S., 1992. Stabilized space–time finite element formulations for unsteady incompressible flows involving fluid body interaction. Ph.D Thesis, University of Minnesota, USA.

Mittal, S., Kumar, V., 1999. Finite element study of vortex-induced cross-flow and in-line oscillations of a circular cylinder at low Reynolds numbers. International Journal of Numerical Methods in Fluids 31, 1087–1120.

Mittal, S., Kumar, V., 2001. Flow-induced oscillations of two cylinders in tandem and staggered arrangement. Journal of Fluids and Structures 15, 717–736.

Mittal, S., Singh, S., 2005. Vortex-induced vibrations at subcritical Re. Journal of Fluid Mechanics 534, 185–194.

Mittal, S., Tezduyar, T.E., 1992. A finite element study of incompressible flows past oscillating cylinders and airfoils. International Journal of Numerical Methods in Fluids 15, 1073–1118.

Norberg, C., 2003. Fluctuating lift on a circular cylinder: review and new measurement. Journal of Fluids and Structures 17, 57–96.

Singh, S.P., Mittal, S., 2005. Vortex-induced oscillations at low Reynolds numbers: hysteresis and vortex shedding modes. Journal of Fluids and Structures 20, 1085–1104.

Stansby, P.K., 1976. The locking-on of vortex shedding due to the cross-stream vibration of circular cylinders in uniform and shear flows. Journal of Fluid Mechanics 74, 641–665.

Tezduyar, T.E., Behr, M., Liou, J., 1992a. A new strategy for finite element computations involving moving boundaries and interfaces—the deforming-spatial-domain/space–time procedure, I: the concept and the preliminary tests. Computer Methods in Applied Mechanics and Engineering 94, 339–351.

Tezduyar, T.E., Behr, M., Mittal, S., Liou, J., 1992b. A new strategy for finite element computations involving moving boundaries and interfaces—the deforming-spatial-domain/space–time procedure, II: computations of free-surface flows, two liquid flows and flows with drifting cylinders. Computer Methods in Applied Mechanics and Engineering 94, 353–371.

Tezduyar, T.E., Mittal, S., Ray, S.E., Shih, R., 1992c. Incompressible flow computations with stabilized bilinear and linear equal-order-interpolation velocity–pressure elements. Computer Methods in Applied Mechanics and Engineering 95, 221–242.

Williamson, C.H.K., Govardhan, R., 2004. Vortex-induced vibrations. Annual Review of Fluid Mechanics 36, 413–455.

Williamson, C.H.K., Roshko, A., 1988. Vortex formation in the wake of an oscillating cylinder. Journal of Fluids and Structures 2, 355–381.